Journal of Photochemistry and Photobiology A: Chemistry 199 (2008) 170–178

Contents lists available at ScienceDirect

Journal of Photochemistry and Photobiology A: Chemistry

journal homepage: www.elsevier.com/locate/jphotochem

Characterization and photoreactivity of N-, S-, and C-doped ZnO under UV and visible light illumination

Lung-Chuan Chen[a], Yi-Jian Tu[a], Yu-Sheng Wang[a], Ruei-Sian Kan[a], Chao-Ming Huang[b,*]

[a] Department of Polymer Materials, Kun-Shan University, Yung Kang City, Tainan 710, Taiwan, ROC
[b] Department of Environmental Engineering, Kun-Shan University, No. 949 Da-wan Road, Yung Kang City, Tainan 710, Taiwan, ROC

ARTICLE INFO

Article history:
Received 17 October 2007
Received in revised form 11 February 2008
Accepted 8 May 2008
Available online 11 June 2008

Keywords:
Zinc oxide
Thiourea
Photocatalyst
Phenol
Acid orange 7
Visible light

ABSTRACT

N-, S-, and C-doped ZnO (N,S,C-ZnO) particles were synthesized from thiourea and zinc sulfate via a precipitation method and were characterized by XRD, XPS, UV–vis spectroscopy, and BET techniques. The photocatalytic activities of the N,S,C-ZnO samples were evaluated by the degradation of acid orange 7 (AO7) and phenol under UV and visible light illumination. XRD results showed that crystallization of the N,S,C-ZnO samples was not well developed after calcination below 700 °C. XPS results suggested that N, S, and C atoms in the samples were predominantly in the bonds of Zn—N, Zn—S and Zn—C after calcination at 500 °C, and were transformed to oxidized forms at 800 °C. UV–vis spectroscopy indicated that dopants N,S,C-species can shift the absorption edge to the visible light region. Incorporating N,S,C-species at appropriate quantities reduced the crystal size and increased the surface area of ZnO samples. The visible light activity of the N,S,C-ZnO samples was confirmed by degradation of phenol. The optimal molar ratios of thiourea to zinc sulfate are 1 and 2 for the highest photocatalytic activities under UV and visible light illumination, respectively. Under visible light illumination, AO7 probably degrades through both the photocatalytic and photosensitized pathways as a result of visible light absorption by N,S,C-ZnO and AO7.

1. Introduction

Photocatalysis is an advanced technology for the degradation of toxic and nonbiodegradable compounds to carbon dioxide and inorganic constituents using semiconductors as catalysts [1]. The photocatalytic process originates from the generation of the charge carriers, electrons (e^-) in the conduction band, and holes (h^+) in the valence band, caused by the photoexcitation of the semiconductors. Some e^-–h^+ pairs escape the recombination process and migrate to the semiconductor surface, where they participate in a series of reactions to form HO• free radicals [1]. HO• free radicals have been widely accepted as the principal oxidizing agents responsible for photocatalytic degradation.

Among the semiconductors applied, titanium dioxide is the most widely employed photocatalytic semiconducting materials because of its chemical inertness, nonphotocorrosion, low cost, and nontoxicity. Although a great deal of effort has been devoted to improving the photocatalytic activity, titanium dioxide suffers from low efficiency under visible light illumination since it has a large band gap energy of 3.2 eV, corresponding to a threshold wavelength of 388 nm. Only approximately 3–5% of the solar energy that reaches the earth can be utilized for photocatalytic reactions when TiO_2 is used as the catalysts [2]. For useful utilization of solar energy, the development of visible light-induced photocatalysts is important. Although numerous attempts have been devoted to preparing solar-driven photocatalysts by doping TiO_2 with transitional and noble metals [3–6], these processes often suffer from thermal instability or an increase in the carrier-recombination centers [6]. Dye-sensitized semiconductors have also been applied to develop visible light catalyzed reactions [7,8]. Unfortunately, they cannot be used in photocatalytic detoxification because the sensitizer may be degraded in the presence of oxygen [9].

Recently, some groups have demonstrated that doping with a nonmetal impurity can provide an effective modification of the electronic structure of TiO_2 and thereby narrowing the band gap [10–18]. Substituting oxygen with nitrogen to form $TiO_{2-x}N_x$ has been shown to be an efficient route to increase visible light photocatalytic activity [10–12]. Fluorine doping shifts the optical absorption edge of TiO_2 to a longer wavelength, and then increases photocatalytic activity in the visible light region [13]. Lettmann et al. [14] prepared visible light active carbon-containing TiO_2 using a sol–gel method. The highly condensed, carbonaceous species formed during calcination is responsible for the photosensitization. Chemically modified carbon-substituted TiO_2 has shown

* Corresponding author. Tel.: +886 6 2050359; fax: +886 6 2050540.
E-mail address: charming@mail.ksu.edu.tw (C.-M. Huang).

1010-6030/$ – see front matter © 2008 Elsevier B.V. All rights reserved.
doi:10.1016/j.jphotochem.2008.05.022

efficient photochemical water splitting under visible light illumination [15,16]. Doping sulfur is also an efficient method for narrowing the band gap energy of TiO_2 and shifts the threshold wavelength to the visible light region [6,17,18].

ZnO is a promising semiconductor material for advanced applications due to its unique chemical and physical properties, environmental stability, and low cost as compared to other binary nanosize metal oxides [19]. The energy levels for the conduction and valence bands, and the electron affinity of zinc oxide are similar to those of TiO_2, making ZnO a likely candidate as a semiconductor material for photocatalysis. It is also anticipated that nanostructured ZnO can become a versatile alternative to TiO_2 since some researchers [20–23] have mentioned that zinc oxide is much more efficient than titanium dioxide, particularly for photocatalytic degradations of azo dyes [20,21], pulp wastewaters [22], and phenols [23] under UV irradiation. Recent studies have also demonstrated that ZnO exhibits more efficiency than TiO_2 in photocatalytic degradation of some dyes under visible light illumination [24]. In addition, ZnO nanocrystals can be applied in hydrogen production and dye-sensitized solar cells with high efficiency [19,25]. However, little attention has been devoted to studying the effect of nonmetal dopants on the photocatalytic activity of ZnO, particularly under visible light illumination [26,27]. Accordingly, the present work attempts to modify ZnO photocatalysts with thiourea to enhance their photocatalytic activity by nonmetal dopants under visible light illumination. The characteristics of the modified ZnO are also examined to relate to the photocatalytic activity. AO7 and phenol are employed as the model contaminants to evaluate the photocatalytic activity of the modified ZnO samples under UV and visible light illumination due to their toxic and nonbiodegradable properties.

2. Experimental

2.1. Preparation of catalysts

N,S,C-ZnO powders were prepared using a precipitation method. Thiourea was mixed with zinc sulfate in 500 ml distillated water to form a 0.25-M aqueous solution. Then, the solution was stirred for 3 h. Following complete dissolution, the solution was treated with an ammonia solution (28%) until the solution pH reached 7. The resulting solution was stirred for another 2 h. Precipitated products were separated from the solution by centrifugation, and dried at 100 °C for 24 h. The obtained products were ground and calcined at an elevated temperature for 3 h with a heating rate of 5 °C/min. The T/Z ratio indicates the molar ratio of thiourea to zinc sulfate. Samples were denoted as TZ0, TZ14, TZ12, TZ11, TZ21, and TZ31 to indicate the T/Z ratios of 0, 1/4, 1/2, 1, 2, and 3, respectively.

2.2. Characterization of photocatalysts

The crystalline phases of the prepared samples were measured by X-ray diffraction (XRD) using a Rigaku D/Max III.V X-ray diffractometer with Cu Kα radiation. The crystal size was assessed from the half-height width of the diffraction peaks using the Scherrer equation. X-ray photoelectron spectra (XPS) were recorded on a Kratos Axis Ultra DLD XPS system. The amounts of the dopants in the modified ZnO are determined by an elemental analyzer (Vario, EL-III). Diffuse reflectance spectroscopy (DRS) was used to determine the threshold wavelength and photoabsorbance of the prepared samples using an UV–vis spectrophotometer (Hitachi, U-3010), equipped with an integrated sphere assembly. The specific surface areas, pore volumes and pore sizes of modified ZnO powders were measured using the Barrett–Emmett–Teller (BET) and Barrett–Joyner–Halenda (BJH) approaches according to the nitrogen adsorption–desorption at 77 K on a Micromeritics ASAP 2020 apparatus.

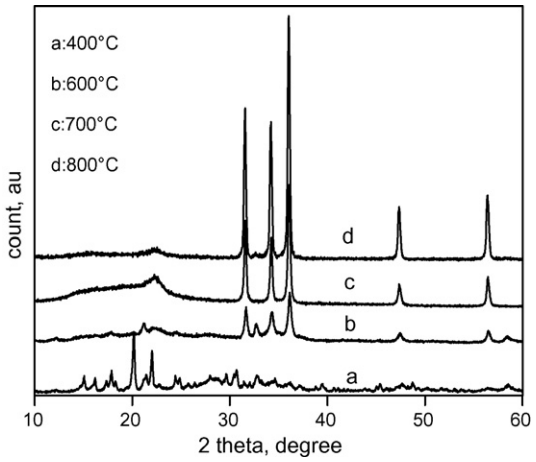

Fig. 1. The XRD spectra of the TZ11 samples at different calcination temperatures.

2.3. Evaluation of photocatalytic activity

Photocatalytic testing was conducted in a thermostatic cylindrical Pyrex reactor with a 500 ml capacity operated at 298 K. A 125-W mercury lamp (HPI 125 W, Philips), with a major emission at 365 nm, was used as the UV light source, and four 10 W white fluorescent light lamps (FL10W-EX, TFC) were used as the visible light source. At the beginning of a run, the desired amount of photocatalyst and 250 ml AO7 solution were fed to the reactor. The solution pH was adjusted by diluted HCl and NaOH solutions. Agitation was produced by a magnetic stirrer rotating fast enough to put the reaction into the region of chemical reaction control. The resulting solution was then stirred continuously in the dark for 60 min to achieve adsorption equilibrium of AO7 on the catalyst. Then, the photocatalytic run was started under UV or visible light illumination. Samples were periodically taken from the reactor, centrifuged at 6000 rpm for 5 min, and then filtered through a 0.22-μm membrane filter before being measured on a UV–vis spectrophotometer (Hitachi, U-3010). Photocatalytic activity was evaluated according to the photoabsorbance of AO7 at the maximum absorption wavelength of 486 nm. The procedure for the photocatalytic degradation of phenol is similar to that for AO7, except that a HPLC system (PerkinElmer, 200S) equipped with a C18 column was used to determine the residual concentration of phenol.

3. Results and discussion

3.1. Characterization of doped ZnO composite

Fig. 1 shows the XRD patterns of the N,S,C-ZnO samples calcined at various temperatures. At 400 °C, a large number of weak and indistinguishable XRD peaks appear, indicating that crystallization is incomplete. However, ZnO and ZnS are suspected to appear in the samples because the diffraction peaks at $2\theta = 31.7°$(100), 34.4°(002), and 36.2°(101), attributed to the former, and those at $2\theta = 26.9°$, 28.5°, 30.6°, 39.6°, and 47.7°, attributed to the latter, are present. According to the JCPDS data (890138, 101255, 721249, 731416), some of the other peaks are suspected to mainly result from S- and OH-containing compounds like $Zn_2(OH)_2SO_4$. When the calcination temperature reached 600 °C, peaks that resulted from the ZnO crystal sharply increased, while the other peaks sig-

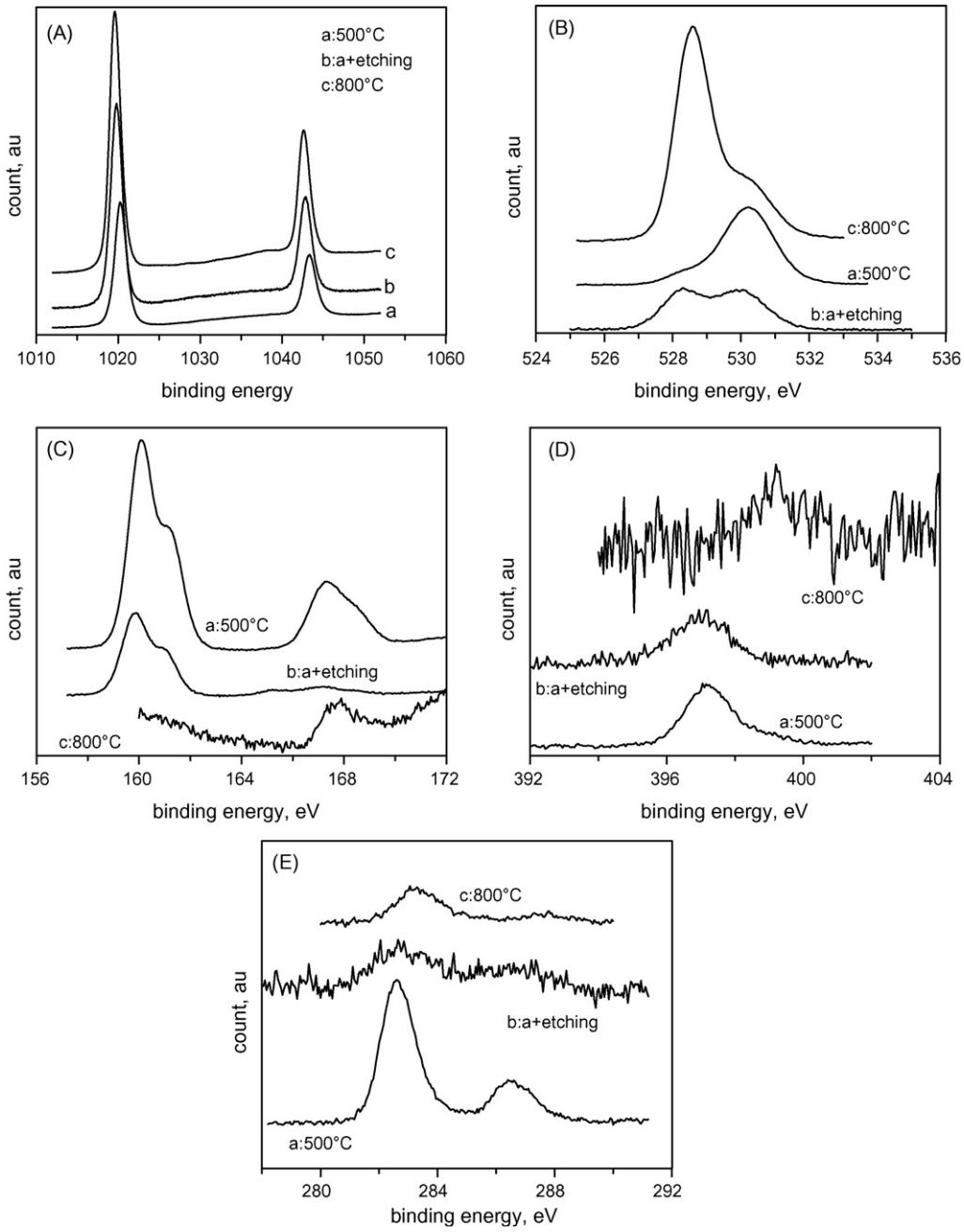

Fig. 2. The XPS spectra of theTZ21 samples at different calcination temperatures. (A) Zn 2p region, (B) O 1s region, (C) S 2p region, (D) N 1s region, and (E) C 1s region; line a: 500 °C, line b: 500 °C after etching, and line c: 800 °C .The peak intensity of the insignificant peak is regulated by timing a factor to make it more observable.

nificantly decreased. The ZnO crystal is in the hexagonal wurtzite phase. Most ZnS in the sample can be oxidized to ZnO and SO_2, which can be removed from the sample or incorporated into the ZnO structure on heating, as shown in the following equation. When the calcination temperature increases to 800 °C, only ZnO crystal peaks can be identified in addition to an unknown peak centered at 22.4°.

$$2ZnS + 3O_2 \rightarrow 2SO_2 + 2ZnO \quad (1)$$

The specific surface areas and pore volumes of the doped ZnO samples are listed in Table 1. When the T/Z ratio of the 500 °C-calcined samples increases from 1/4 to 2, the specific surface area and pore volume increase from 1.9 to 20.5 m^2/g and 0.008 to 0.046 ml/g, respectively. Further increasing the T/Z ratio to 3 decreases the specific surface area and pore volume to 11.6 m^2/g and 0.034 ml/g, respectively. For the TZ11 samples, increasing calcination temperature from 400 to 700 °C increases the surface area from 5.5 to 8.3 m^2/g, which then decreases to 4.5 m^2/g when the calcination temperature reaches 800 °C. It is suggested that ZnS forms in addition to ZnO after calcination at lower calcination temperature. At low T/Z ratios, the predominant product, ZnO crystal, grows effectively, and then exhibits low surface area. As the T/Z ratio increases, the quantity of ZnS increases, which prevents the growth of ZnO crystal since both the sintering between particles and the growth of the ZnO crystalline through a surface diffusion mechanism are suppressed because of the dissimilar boundaries between ZnS and ZnO [28], therefore, the surface area increases. When the T/Z ratio reaches 3, a lot of ZnS and other N-, S-, and C-containing

Table 1
Specific surface areas, pore sizes, pore volumes, and crystal sizes of doped ZnO with T/Z ratios and calcination temperatures

Sample	Calcination temperature (°C)	T/Z ratio	Specific surface area (m^2/g)	Pore volume (ml/g)	Crystal size (nm)
TN11	800	1/1	4.5	0.009	31.6
TZ11	700	1/1	8.3	0.022	29.3
TZ11	600	1/1	7.2	0.024	
TZ11	500	1/1	7.4	0.017	
TZ11	400	1/1	5.5	0.015	
TN14	500	1/4	1.9	0.008	
TZ12	500	1/2	5.5	0.017	
TZ21	500	2/1	20.5	0.046	
TZ31	500	3/1	11.6	0.034	

species are possibly adsorbed on the surface of ZnO, diminishing the pore size and the pore volume, and leading to a decrease in the surface area. This mechanism is also suspected to account for the surface area of the 400 °C-calcined sample being lower than that at 500 °C, which goes against the general rule that a metal oxide's surface area decreases with increasing calcination temperature. Chemical reactions of N,S,C-species adsorbed on ZnO with increasing calcination temperature may also explain the results. Calcination of doped ZnO at 800 °C can result in noticeable sintering effect and/or grain growth of the doped ZnO sample; consequently, the surface area decreases.

The chemical states of the atoms in the samples are examined by XPS before and after etching by Ar^+ sputtering. The XPS survey shows that N, S and C atoms are all present and are incorporated into the bulk phase of the sample after calcination at temperature higher than 500 °C. Fig. 2(A) shows the spectra for the Zn 2p region. Binding energies around 1020 and 1043 eV are assigned to Zn 2p3 and 2p1 electrons, respectively, indicating Zn is in the 2+ state [27,29,30]. Both binding energies slightly decrease with increasing calcination temperature from 500 to 800 °C and the etching process, which can be attributed to the change of bond structures between Zn and other atoms existed in the samples. Jung et al. [29] have demonstrated that Zn binding energy in ZnS is larger than that in ZnO. In this work, the ratio in amount of ZnS/ZnO after calcination at 500 °C is larger than that at 800 °C; therefore, a lower binding energy is expected with increasing calcination temperature. The experimental results also imply that more dopants are present on the surface than in the bulk phase of the sample.

The XPS depicted in Fig. 2(B) shows the high-resolution O 1s region, in which the peaks centered at 528.5 and 530.5 eV are observed and are the predominant binding energies for O atom in the 500- and 800 °C-calcined samples, respectively. It is considered that some S, C and N atoms may bound to oxygen in the sample, however, their contents decrease with increasing temperature, causing more Zn—O bonds appear at 800 °C than that at 500 °C. Hence, the peak at 528.5 eV can be assigned to O bound to Zn atom, and that at 530.5 eV can be attributed to O bound to S, N or C atom. It is expected that surface hydroxyl groups also contribute to the peak at 530.5 eV. Similar results were also reported by Duran et al. [30], who studied the oxidation of ZnS.

Fig. 2(C) shows the high-resolution XPS spectra of the S 2p region in the samples. Two main bands centered at 160 and 167.5 eV occur, and can be deconvoluted into four peaks near 159.8, 161.0, 167.5, and 168.7 for the sample calcined at 500 °C. The first two peaks can be attributed to S^{2-} and the last two can be assigned to S^{4+} and/or S^{6+} according to the data reported in the literature [17,18,31,32]. Etching the sample reduces the XPS intensity, suggesting the quantity of sulfur species on the surface is larger than that in the bulk phase. As calcination temperature increases to 800 °C, most sulfur atoms escape from the sample, and the band centered at 160.0 eV disappears, only the band centered at 168.0 eV remains, implying sulfur atoms are all in the 4+ and/or 6+ state.

Fig. 2(D) shows the high-resolution XPS spectra of N 1s region. A main peak centered at 397.0 eV for the 500 °C-calcined sample is obtained, which can be ascribed to N atom in Zn—N bond. In addition, a peak around 399.3 eV, superimposed with that at 397.0 eV, can also be detected, which is suggested to result from N atom in the Zn—O—N bond [12,33–36]. Calculation at 800 °C significantly reduces the content of N atom in the sample, and the peak at 397.0 eV completely disappears, while the peak at 399.3 eV remains. In addition, it seems that insignificant peaks around 400.5, 401.5, and 402.5 eV also appear. These results indicate that nitrogen is in the oxidized forms after being calcined at 800 °C.

Fig. 2(E) shows the high-resolution XPS spectra C 1s region. Two peaks around 282.5 and 286.7 eV are observed, which are suspected to arise from C in Zn—C and Zn—O—C bonds [31,32] for the 500 °C-calcined sample. When the calcination temperature increases to 800 °C, the main binding energy of C 1s slightly shifts from 282.5 to 283.2 eV. An oxidized form of carbon can be anticipated to account for this change.

The amounts of N, S, and C in the samples are determined by the elemental analysis and are shown in Table 2. The results demonstrate that increasing the T/Z ratio increases the amounts of N and C, and decrease the amount of S in the samples. In the absence of thiourea, N and S are expected to be inherent from the precursors of ammonium water and zinc sulfate, while carbon is suspected to

Table 2
Content of N, S, and C atoms in the prepared samples

Sample[a]	Calcination temperature (°C)	Composition (wt%)					
		Bulk[b]			Surface[c]		
		N	S	C	N	S	C
TZ0	800	0.045	5.567	0.023	0.110	10.73	0.033
TZ12	800	0.072	0.625	0.031	0.141	0.516	0.049
TZ21	800	0.116	0.264	0.091	0.237	0.190	0.107
TZ21	500	1.565	20.34	0.747	1.73	15.43	0.805

[a] Sample was cleaned by ultrasonic vibration for 10 min and washing by water.
[b] Determined by elemental analyzer.
[c] Determined by XPS before etching.

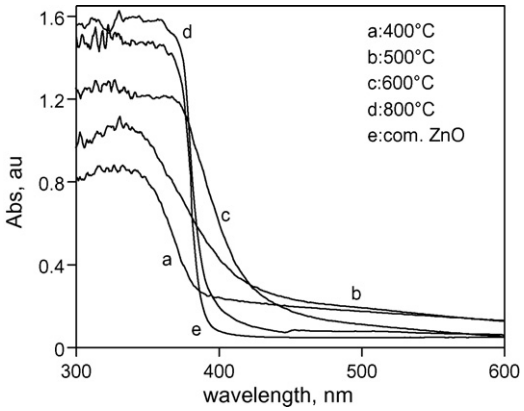

Fig. 3. The UV–vis diffuse reflectance spectra of the TZ11 samples at different calcination temperatures.

be from the impurity in the starting materials or carbon dioxide in air. It seems that increasing the amount of thiourea can increase and decrease the doping levels of S^{2-} and S^{4+} or S^{6+} in the samples, respectively; S^{2-} is supposed to be more easily removed from the sample during calcination at 800 °C when compared with N and C, leading to a maximum and a minimum sulfur contents are observed for the 800 °C-calcined samples with T/Z ratios of 0 and 2, respectively.

Fig. 3 shows the UV–vis diffuse reflectance spectra of the N,S,C-ZnO samples at different calcination temperatures. The absorbance shoulders significantly shift from the UV to the visible light region for the N,S,C-ZnO samples. The 500 °C-calcined sample exhibits strong photoabsorption in the visible light region when compared with other samples. A notable decrease in photoabsorption in the visible light region for the doped ZnO is obtained when the calcination temperature reaches 800 °C, but it still exhibits a larger photoabsorbance than pure commercial ZnO does. The amounts of N,S,C-species in the 400 °C-calcined sample are larger than those calcined at higher temperatures. However, some of the N,S,C-species are likely to only remain on the ZnO surface, and cannot contribute to the visible light sensitivity. Therefore, the photoabsorbance shoulder is around 390 nm, which is not markedly different from that of ZnO. Increasing the calcination temperature to 500 °C enhances incorporation of N,S,C-species into the ZnO structure and reduces the remained N,S,C-species, shifting the photoabsorbance shoulder to the visible light region. A reduction in surface area and escape of the incorporated N,S,C-species are two possible causes of the lower photoabsorption in the visible light region as the calcination temperature further increases to 800 °C.

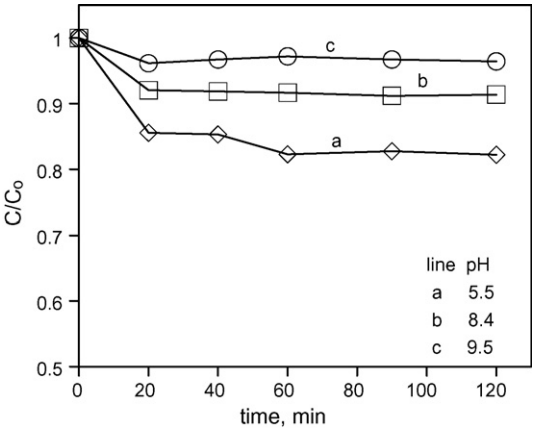

Fig. 4. Adsorption of AO7 on the 800 °C-calcined TZ11 sample in the dark. Volume of AO7 solution: 250 ml, initial AO7 concentration: 20.0 ± 0.5 ppm, and catalyst load: 1 g/l.

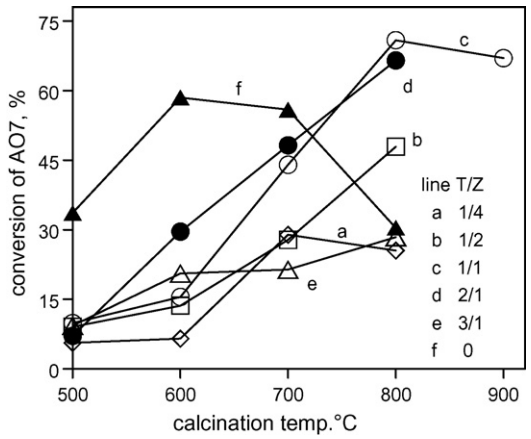

Fig. 5. Plot of AO7 conversion against calcination temperature for the prepared samples as a function of the T/Z ratio under UV illumination. Catalyst dosage: 1 g/l, initial pH: 6.6, initial AO7 concentration: 20.0 ± 0.5 ppm, volume of solution: 250 ml, and stir rate: 600 rpm.

3.2. Adsorption of AO7 on N-, S-, C-doped ZnO

Adsorption of AO7 on the 800 °C-calcined TZ11 sample was carried out in the dark at room temperature. Fig. 4 shows the normalized residual concentration of AO7 varied with adsorption time at initial pHs of 5.5, 8.4, and 9.5. It can be observed that most adsorption occurs within 60 min. Increasing pH from 5.5 to 9.5 decreases the equilibrium adsorption amount of AO7 from 3.56 to 0.71 mg/g. This trend correlates well with an anion substrate such as AO7 dye. Photolysis of AO7 illuminated by UV or visible light in the absence of a photocatalyst was also performed. Less than 2.0% of the original AO7 was decolorized after 3 h of illumination, implying neither UV nor visible light can bring about the photolysis of AO7.

3.3. Photocatalytic degradation of AO7 under UV illumination

Fig. 5 shows the photocatalytic conversion of AO7 affected by the calcination temperature and T/Z ratio of the N,S,C-ZnO samples under UV illumination. The optimal calcination temperature for photocatalytic activity is 800 °C for all T/Z ratios examined, except for the sample with a T/Z ratio of 1/4, which is at 700 °C. The sample with T/Z of 1 calcined at 800 °C shows the highest photocatalytic activity among the T/Z ratios and calcination temperatures evaluated. One possible explanation is that the crystalline extent of ZnO substantially influences photocatalytic activity. N,S,C-dopants can interfere with the crystallization of ZnO, which is an important factor affecting UV absorption and transport of the photogenerated charge carriers; therefore, elevating calcination temperature up to 800 °C can improve photocatalytic activity. Increasing the T/Z ratio from 1/4 to 1 increases AO7 conversion for 2 h illumination from 25.5 to 70.9%, and further increasing the T/Z ratio to 3 decreases AO7 conversion to 39.6% for the 800 °C-calcined sample. The discrepancy in photocatalytic activity caused by the T/Z ratio is insignificant at low calcination temperatures due to the low crystallization level of N,S,C-ZnO. Increasing the amount of thiourea decreases the total quantity of the N, S, C atoms in the 800 °C-calcined sample as shown in Table 2. It is considered that the photocatalytic efficiency can be improved in the presence

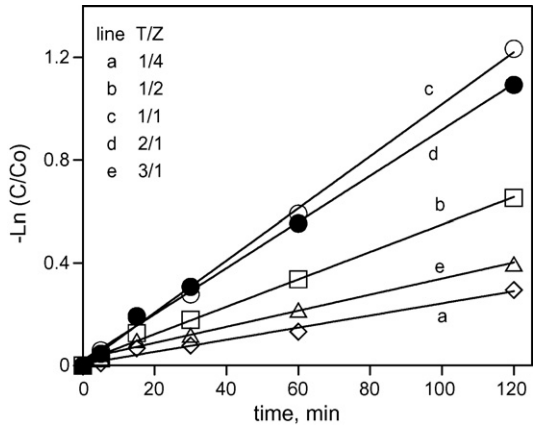

Fig. 6. Logarithmic plot of the normalized AO7 concentration against reaction time for the prepared samples with varying T/Z ratios under UV illumination. Catalyst dosage: 1 g/l, initial AO7 concentration: 20.0 ± 0.5 ppm, volume of solution: 250 ml, and stir rate: 600 rpm.

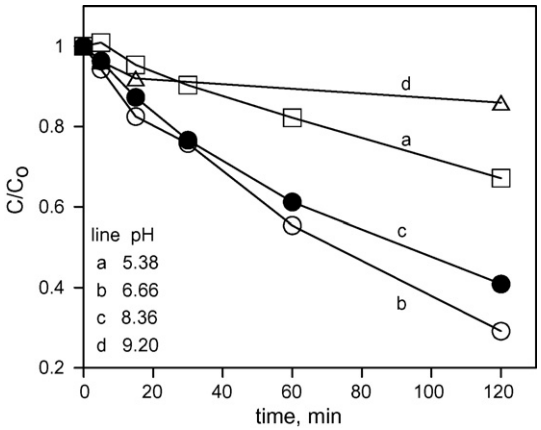

Fig. 7. Effect of initial pH on the photocatalytic conversion of AO7 under UV illumination. Catalyst dosage: 1 g/l, T/Z ratio: 1, volume of solution: 250 ml, stir rate: 600 rpm, and initial AO7 concentration: 20.0 ± 0.5 ppm.

of a trace amount of dopants by reducing the recombination of e^-–h^+ pairs; however, an excess amount of dopants may reduce the absorption of the incident UV illumination, increase the crystal defects and even act as the e^-–h^+ recombination centers, decreasing the photocatalytic activity. Accordingly, an optimal T/Z ration of 1 is accomplished to attain the maximum photocatalytic efficiency under UV illumination.

Usually, photocatalytic reactions follow the Langmuir–Hinshelwood adsorption model, which can be simplified to a pseudo first-order kinetic model at a low substrate concentration [1]. Fig. 6 shows the normalized logarithmic plot of AO7 concentration against the irradiation time. Using regression fit techniques, straight lines are attained, and their slopes correspond to the apparent rate constant, k_{app}, according to the equation $\ln(Co/C) = k_{app}t$, where Co and C indicate the AO7 concentrations at times 0 and t, respectively. Table 3 summaries the calculated k_{app} and the corresponding R^2 values. The maximum and minimum apparent rate constants are 0.010 and 0.0024 min^{-1} with T/Z ratios of 1 and 1/4, respectively. The R^2 values are all close to 1.0, implying that the experimental data are consistent with the pseudo first-order kinetic model.

The impact of pH on the decolorization efficiency of AO7 was studied in the pH range of 5.38–9.20. Increasing pH from 5.38 to 6.66 increases the AO7 conversion for a 2-h run from 32.9 to 70.9%. Further increasing pH to 9.20 decreases the conversion to 15.0%, as shown in Fig. 7. The optimum pH for this system is close to 7.0. A low pH will be beneficial for the adsorption of AO7 on the catalyst; however, it will be harmful for formation of HO• free radicals. Accordingly, an optimum pH can be used to obtain the highest photocatalytic activity.

Table 3
Apparent rate constants (k_{app}) with T/Z ratios of the 800 °C-calcined samples under UV and visible light illumination

T/Z ratio	k_{app}[a] (min^{-1})	
	UV	Visible light
1/4	0.0024 (0.982)	0.0015 (0.987)
1/2	0.0053 (0.995)	–
1	0.010 (0.997)	0.0042 (0.976)
2	0.009 (0.997)	0.0083 (0.997)
3	0.0035 (0.968)	0.0063 (0.967)

[a] Number in the parentheses is R^2.

3.4. Photocatalytic degradation of phenol under visible light illumination

Phenol in aqueous solution is applies as the model contaminant to evaluate the photocatalytic activity of the N-, S-, and C-doped ZnO samples under visible light irradiation. Fig. 8 shows the effect of the calcination temperature of the TZ21 sample on the conversion of phenol with irradiation time. Increasing calcination temperature from 500 to 800 °C increases the conversion from 13.9 to 31.5%. Although the 500 °C-calcined sample exhibits the highest photoabsorption in the visible light region, however, a lowest visible light activity is revealed. At 500 °C, more N, S, and C are present in the sample and contribute to the visible light absorption, however, they retard the crystallization development of the sample, causing low photocatalytic activity due to a high recombination rate of e^- and h^+. In addition, changing of chemical states of N and S may be another factor affecting the dependence of photocatalytic activity with calcination temperature. At 500 °C, most N and S are in the forms of Zn–N and Zn–S, and they change to Zn–O–N and Zn–O–S after calcination at 800 °C. Asahi et al. [37] ascribed the visible light activity of N-doped TiO_2 to the formation of Ti—N bonds, Wang et al. [12] pointed out that only N—Ti—O bond can extend the optical absorption of TiO_2 to visible light region for the $TiO_{2-x}N_x$ sample. However, Sato et al. [34] cited many references

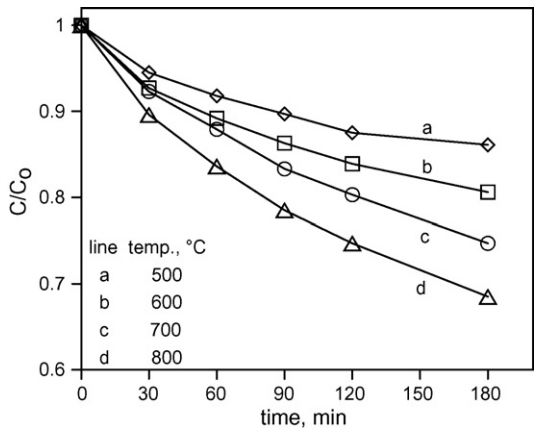

Fig. 8. Effect of calcination temperature of the TZ21 samples on the photocatalytic conversion of phenol under visible light illumination. Catalyst dosage: 1 g/l, initial phenol concentration: 10.0 ± 0.5 ppm, pH: 6.6, volume of solution: 250 ml, and stir rate: 600 rpm.

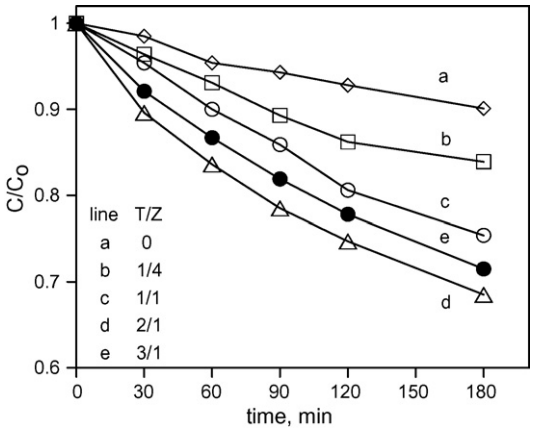

Fig. 9. Effect of the T/Z ratio of the 800 °C-calcined samples on the photocatalytic conversion of phenol under visible light illumination. Catalyst dosage: 1 g/l, initial phenol concentration: 10.0 ± 0.5 ppm, pH: 6.6, volume of solution: 250 ml, and stir rate: 600 rpm.

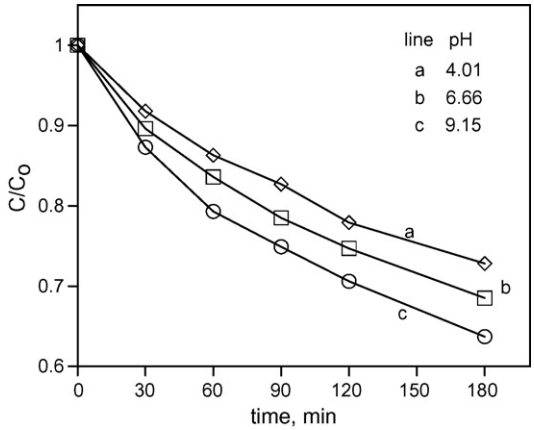

Fig. 10. Effect of initial pH on the photocatalytic degradation of phenol over 800 °C-calcined TZ21 samples under visible light illumination. Catalyst dosage: 1 g/l, initial phenol concentration: 10.0 ± 0.5 ppm, volume of solution: 250 ml, and stir rate: 600 rpm.

and concluded that N doped in TiO_2 without Ti—N bonding is also responsible for visible light activity. Gole et al. [35] reported that Ti–O–N-based catalysts also showed visible light activity. As far as we know, no detail study about the relation between the structure of N bounded to ZnO and visible light activity was reported [26]. Both anionic and cationic S-doped TiO_2 samples were reported to show visible light activity [17,18,31,32]. Recently, Kim et al. [27] synthesized ZnO_xS_{1-x} samples and indicated an enhancement in the visible light activity when compared with pure ZnO samples. An elevation in the visible light activity by doping carbon on TiO_2 has been also reported in the literature [14–16]. In view of these reports, it is expected that doping N, S, or C atom can show a promotion influence on the visible light activity of ZnO, however, the extent of the doping-effect may change with calcination temperature due to the changes of chemical states of the dopants and physical properties of doped ZnO samples, such as the level of crystallization.

The photocatalytic conversion of phenol increases from 9.9 to 31.5% as the T/Z ratio increases from 0 to 2, further increasing the ratio to 3, however, decreases the conversion to 28.5% as shown in Fig. 9. Increasing the T/Z ratio increases the amounts of N- and C-species, and decreases the S-species in the 800 °C-calcined sample. Hence, it seems that N and/or C show a more promotive influence on the visible light activity than S; however, S-dopants also show positive effect on raising photocatalytic activity, causing the sample with T/Z ratio of 3 reveals lower activity than that of 2. Zaleska et al. [31] studied N-, S-, and C-doped TiO_2 and pointed out the catalytic activity could be associated to the highest content of sulfur and nitrogen and only moderate amount of carbon; however, the interaction effect of these dopants were not systematically studied. In this work, increasing the amount of thiourea increases the content of nitrogen and carbon, but decrease the content of sulfur in the samples calcined at 800 °C. Therefore, an appropriate amount of thiourea is required to attain the optimum photocatalytic activity under visible light illumination.

Fig. 10 shows the effect of pH on the photocatalytic degradation of phenol under visible light illumination. Increasing pH from 4.01 to 9.15 increases the conversion from 27.2 to 36.3%. The results indicate that pH of 9.15 exhibits the highest activity, which is different from the pH of 6.66 for AO7 under UV illumination. One possible interpretation for this discrepancy is that the generation of $HO^{\bullet}$ free radicals from h^+ and OH^- rather than the adsorption of substrates on the photocatalyst plays an important role in affecting photocatalytic reaction.

3.5. Photocatalytic degradation of AO7 under visible light illumination

Fig. 11 shows the time evolution of AO7 concentration during the photocatalytic reaction under visible light illumination. About 43.3, 20.5, 32.1, and 77.8% of the original AO7 were photodegraded for the TN21 samples calcined at 500, 600, 700, and 800 °C, respectively, after a 3-h illumination. The 800 °C-calcined sample exhibits the most visible light photocatalytic activity despite having the smallest surface area and the lowest visible light photoabsorption. Fig. 12 shows the photocatalytic activities of the samples prepared with different T/Z ratios after calcination at 800 °C. Increasing the T/Z ratio from 1/4 to 2 increases the AO7 conversion from 23.3 to 77.8%; however, it decreases to 69.2% when the T/Z ratio is further increased to 3.

The visible light catalytic activity of the TN21 sample with respect to calcination temperature decreases in the order of 800 > 500 > 700 > 600 °C; however, that for phenol is in the order of 800 > 700 > 600 > 500 °C. AO7 can follow a photosensitized process by absorbing visible light to become excited, and then inject electrons to the conduction band of semiconductors. The injected electrons on the semiconductor can reduce adsorbed oxygen to superoxide free radicals, $O_2^{\bullet -}$, followed by a series reaction to pro-

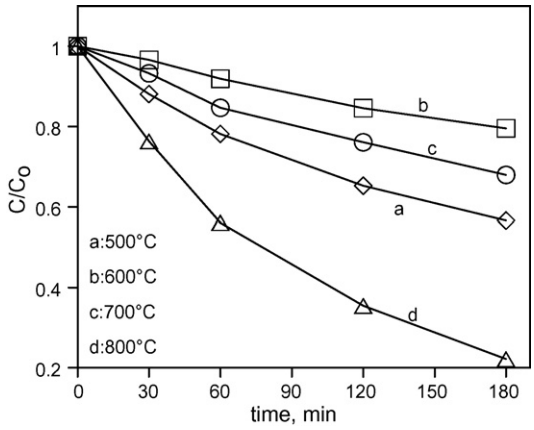

Fig. 11. Effect of calcination temperature of the TZ21 samples on the photocatalytic conversion of AO7 under visible light illumination. Catalyst dosage: 1 g/l, initial AO7 concentration: 20.0 ± 0.5 ppm, pH: 6.6, volume of solution: 250 ml, and stir rate: 600 rpm.

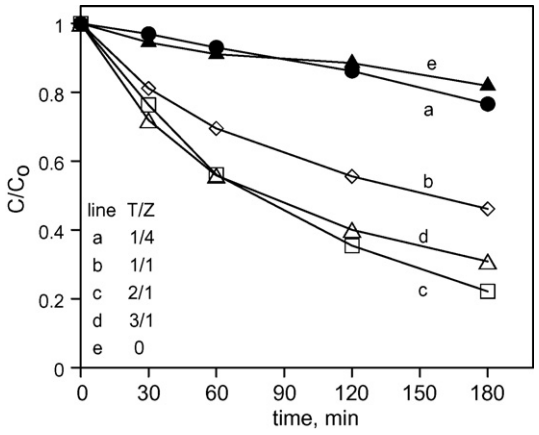

Fig. 12. Effect of the T/Z ratio of the 800 °C-calcined samples on the photocatalytic conversion of AO7 under visible light illumination. Catalyst dosage: 1 g/l, initial AO7 concentration: 20.0 ± 0.5 ppm, pH: 6.6, volume of solution: 250 ml, and stir rate: 600 rpm.

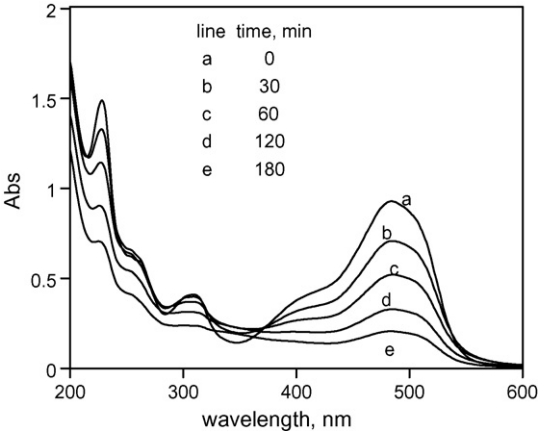

Fig. 13. The temporal evolution of the absorption spectra of AO7 during photocatalytic reaction under visible light illumination. pH: 6.6, initial AO7 concentration: 20.0 ± 0.5 ppm, T/Z ratio: 2/1, catalyst dosage: 1 g/l, and volume of solution: 250 ml.

duce hydrogen peroxide and HO• free radicals [38], enhancing the photocatalytic efficiency. We are of the opinion that photosensitized reaction leads to a higher photodegradation of AO7 at 500 °C when compared with those at 600 and 700 °C.

Fig. 13 shows the temporal evolution of the absorption spectra of AO7 during photocatalytic degradation under visible light illumination. Subsequent illumination causes a continuous decrease of the UV and visible bands of AO7 with increasing irradiation time, which is not accompanied by new absorption peaks during the run. These results support the hypothesis that intermediates formed during photocatalytic reactions can be successfully photodegraded by further illumination. Approximately 52.3, 37.9, and 41.5% decreases in the absorbances at 227, 253, and 308 nm are obtained at 180 min, as shown in Fig. 13. Furthermore, the decreases in absorbances at 253 and 308 nm in the final stage of 120–180 min of the run are more significant than those in the initial stage of 0–120 min. These results strongly suggest that N,S,C-ZnO can be used for a complete mineralization of AO7 under visible light illumination.

4. Conclusions

N,S,C-species can be incorporated into the bulk phase to form N-, S-, and C-doped ZnO. Chemical states of the N,S,C-dopants change with calcination temperature, and are likely to be in the oxidized forms after calcination at 800 °C. Sulfur atoms in the 500 °C-calcined sample are mainly in the -2 state, and transformed to 4+/6+ states after calcination at 800 °C. S-species are easier to be removed from the sample than those of N and C after calcination at 800 °C. Crystallization of ZnO is greatly suppressed due to N,S,C-dopants and not well developed after calcination below 700 °C. The 500 °C-calcined N,S,C-ZnO show strong photoabsorbance in the visible light region. An appropriate amount of dopants can reduce the recombination of $e^- - h^+$ pairs and raise the photocatalytic activity under UV illumination. The amounts and chemical states of the dopants, and extent of crystallization of the samples are the predominant factors affecting the photocatalytic degradation of phenol under visible light illumination. The photosensitized reaction resulted from the visible light absorption by AO7 is suggested to cause the 500 °C-calcined sample showing a high photocatalytic activity when compared with those at 600 and 700 °C in photodegradation of AO7. The optimal T/Z ratios to obtain the maximum photocatalytic activities under UV and visible light illumination are 1 and 2, respectively.

Acknowledgements

The authors would like to thank the National Science Council of Taiwan, the Republic of China, for financially supporting this work under Contract No. NSC-94-2745-E-168-005-URD. The authors also thank Professor Tai-Chou Lee, National Chung Cheng University, for the kind assistance in XPS analysis.

References

[1] O. Carp, C.L. Huisman, A. Reller, Prog. Solid Sate Chem. 32 (2004) 22.
[2] Y.M. Lin, Y.H. Tseng, J.H. Huang, C.C. Chen, I. Wang, Environ. Sci. Technol. 40 (2006) 1616.
[3] J. Moon, H. Tajagi, Y. Fujishiro, M. Awano, J. Mater. Sci. 36 (2001) 949.
[4] J.M. Herrmann, H. Tahiri, Y. Ait-Ichou, Appl. Catal. B 13 (1997) 219.
[5] M. Anpo, M. Takeuchi, J. Catal. 216 (2003) 505.
[6] T. Umebayashi, T. Yamaki, S. Yamamoto, A. Miyashita, S. Tanaka, T. Sumita, K. Asai, J. Appl. Phys. 93 (2003) 5156.
[7] F. Kiriakidou, D.I. Kondarides, K.E. Verykios, Catal. Today 54 (1999) 119.
[8] J.C. Yu, Y. Xie, H.Y. Tang, L. Zhang, H.C. Chan, J. Zhao, J. Photochem. Photobiol. A: Chem. 156 (2003) 235.
[9] H. Kisch, W. Macyk, Chem. Phys. Chem. 3 (2002) 399.
[10] C.M. Huang, L.C. Chen, K.W. Cheng, G.T. Pan, J. Mol. Catal. A: Chem. 261 (2007) 218.
[11] R. Nakamura, T. Tanaka, Y. Nakato, J. Phys. Chem. B 108 (2004) 10617.
[12] X. Wang, J.C. Yu, Y. Chen, L. Wu, X. Fu, Environ. Sci. Technol. 40 (2006) 2369.
[13] J.C. Yu, J. Yu, W. Ho, W. Ho, W. Ho, Z. Jiang, Chem. Mater. 14 (2002) 3808.
[14] C. Lettmann, K. Hildenbrand, H. Kisch, W. Macyk, W.F. Maier, Appl. Catal. B 32 (2001) 215.
[15] N. Nagaveni, M.S. Hegde, N. Ravishankar, G.N. Subbanna, G. Madras, Langmuir 20 (2004) 2900.
[16] S.U.M. Khan, M. Al-Shahry, W.B. Ingler Jr., Science 297 (2002) 2243.
[17] T. Ohno, M. Akiyoshi, T. Umebaysshi, K. Asai, T. Mitsui, M. Matsumura, Appl. Catal. A: Gen. 265 (2004) 115.
[18] T. Ohno, T. Tsubota, Y. Nakamura, K. Soyama, Appl. Catal. A: Gen. 288 (2005) 74.
[19] K.G. Kanade, B.B. Kale, J.-O. Baeg, S.M. Lee, C.W. Lee, S.-J. Moon, H. Chang, Mater. Chem. Phys. 102 (2007) 98–104.
[20] A. Akyol, H.C. Yatmaz, M. Bayramoglu, Appl. Catal. B: Environ. 54 (2004) 19.
[21] N. Daneshvar, D. Salari, A.R. Khataee, J. Photochem. Photobiol. A: Chem. 162 (2004) 317.
[22] M.C. Yeber, J. Rodriguez, J. Freer, J. Baeza, N. Duran, H.D. Mansilla, Chemosphere 39 (1999) 10.
[23] A.A. Khodja, T. Sehili, P.J.F. ihichowski, P. Boule, J. Photochem. Photobiol. A 141 (2001) 231.
[24] F. Peng, H. Wang, H. Yu, S. Chen, Mater. Res. Bull. 41 (2006) 2123.
[25] E. Keis, H. Magnusson, S.E. Lindstrom, A. Lindquist, Hagfeldt, Sol. Energy Mater. Sol. Cells 73 (2002) 51.
[26] D. Li, H. Haneda, J. Photochem. Photobiol. A: Chem. 155 (2003) 171.
[27] C. Kim, S.J. Doh, S.G. Lee, S.J. Lee, H.Y. Kim, Appl. Catal. A: Gen. 330 (2007) 127.
[28] Wang, X. Wang, B.-Q. Xu, J. Zhao, B. Mai, P. Peng, G. Sheng, J. Fu, J. Photochem. Photobiol. A: Chem. 168 (2004) 47.
[29] J.W. Jung, H.C. Lee, J.S. Wang, This Solid Films 290/291 (1996) 18.
[30] J.D.G. Duran, M.C. Guindo, A.V. Delgado, J. Colloid Interface Sci. 173 (1995) 436.

[31] A. Zaleska, P. Gorska, J.W. Sobceak, J. Hupka, Appl. Catal. B: Environ. 76 (2007) 1.
[32] H. Sun, Y. Bai, Y. Cheng, W. Jin, N. Xu, Ind. Eng. Chem. Res. 45 (2006) 4971.
[33] Y.F. Mei, R.K.Y. Fu, G.G. Siu, K.W. Wong, P.K. Chu, R.S. Wang, H.C. Ong, Appl. Surf. Sci. 252 (2006) 8131.
[34] S. Sato, R. Nakamura, S. Abe, Appl. Catal. A: Gen. 284 (2005) 131.
[35] J.L. Gole, J.D. Stout, C. Burda, Y. Lou, X. Chen, J. Phys. Chem. B 108 (2004) 1230.
[36] P. Wu, J. Tang, Z. Dang, Mater. Chem. Phys. 103 (2007) 264.
[37] R. Asahi, T. Morikawa, T. Ohwaki, K. Aoki, Y. Taga, Science 293 (2001) 269.
[38] M. Stylidi, D.I. Kondarides, X.E. Verykios, Appl. Catal. B: Environ. 47 (2004) 189.